A structural subgrid-scale model for relative dispersion in large-eddy simulation of isotropic turbulent flows by coupling kinematic simulation with approximate deconvolution metho...

Article *in* Physics of Fluids · November 2018

DOI: 10.1063/1.5049731

CITATION
1

READS
102

3 authors:

Zhideng Zhou
Chinese Academy of Sciences
4 PUBLICATIONS **6** CITATIONS
SEE PROFILE

Shizhao Wang
Chinese Academy of Sciences
41 PUBLICATIONS **312** CITATIONS
SEE PROFILE

Guodong Jin
Chinese Academy of Sciences
39 PUBLICATIONS **368** CITATIONS
SEE PROFILE

This manuscript was accepted by Phys. Fluids. Click here to see the version of record.

A structural subgrid-scale model for relative dispersion in large-eddy simulation of isotropic turbulent flows by coupling kinematic simulation with approximate deconvolution method

Zhideng Zhou (周志登),[1,2] Shizhao Wang (王士召),[1,2] and Guodong Jin (晋国栋)[1,2,a)]

[1)] *The State Key Laboratory of Nonlinear Mechanics, Institute of Mechanics, Chinese Academy of Sciences, Beijing 100190, China*

[2)] *School of Engineering Sciences, University of Chinese Academy of Sciences, Beijing 100049, China*

(Dated: 7 October 2018)

A kinematic simulation with an approximate deconvolution (KSAD) hybrid model is proposed to predict the Lagrangian relative dispersion of fluid particles in a large eddy simulation (LES) of isotropic turbulent flows. In the model, a physical connection between the resolved and subgrid scales is established through the energy flux rate at the filter width scale. Due to the lack of subgrid-scale (SGS) turbulent structures and SGS model errors, the LES cannot accurately predict the two- and multi-point Lagrangian statistics of the fluid particles. To improve the predictive capability of the LES, we use an approximate deconvolution model (ADM) to improve the resolved scales near the filter width and a kinematic simulation (KS) to recover the missing velocity fluctuations beneath the subgrid scales. To validate the proposed hybrid model, we compare the Lagrangian statistics of two- and four-particle dispersion with the corresponding results from the direct numerical simulation (DNS) and the conventional LES. It is found that a significant improvement in the prediction of the Lagrangian statistics of fluid particles is achieved through the KSAD hybrid model. Furthermore, a parametric study regarding the wavenumbers and orientation wavevectors is conducted to reduce the computational cost. Good results can be obtained using a small number of wavenumber modes and orientation wavevectors. Thus, we can improve the prediction of the Lagrangian dispersion of fluid particles in the LES by applying the KSAD hybrid model at an acceptable computational cost.

[a)] Corresponding author: gdjin@lnm.imech.ac.cn

I. INTRODUCTION

In recent years, numerical simulation methods have been applied to study particle-laden turbulent flows, which occur frequently in environmental applications and industrial processes. Direct numerical simulation (DNS) emerges as a powerful research tool which can resolve all of the turbulent scales and accurately predict particle statistics. Because the instantaneous range of the space and time scales in turbulent flows rapidly increases with an increasing Reynolds number, it is too expensive for the DNS of practical flows at high Reynolds numbers[1]. As a compromise, large eddy simulation (LES) can resolve the turbulent flow fields at a coarser grid resolution and directly compute the large, energy-containing scales, while the effects of the subgrid scales on the large-scale ones need to be modeled through a subgrid-scale (SGS) model. A variety of closure models have been developed for the LES of different kinds of flows[2–12]. The performance of eddy-viscosity models such as QR, Wall-Adapting Local Eddy-viscosity (WALE)[13], and the S3PQR models[4] is assessed using DNS data of Rayleigh-Benard convection. It shows that these models can well describe the effects of SGS motions on the resolved scales, but fail to exactly describe the SGS heat flux and the enstrophy. The tensor-diffusivity approach is proposed to model the SGS heat flux[3]. The SGS characteristic length in the eddy-viscosity models for LES is proposed based on the representations of SGS stress tensor. The model can minimize the effects of mesh anisotropies on the results of turbulence simulations on unstructured meshes[5]. A dynamic model based on SGS dissipation is proposed based on the Germano identity[2]. The model coefficients are determined by minimizing the square error of the resolved dissipation rate. The model can give more accurate results about the physical quantities than traditional dynamic mixed model[6]. Further, the scale-adaptive dynamic Smagorinsky-Lilly model and mixed nonlinear model based on physical constraints are proposed by the same authors. The resulting models can effectively incorporate the viscous effect near the wall and give much better results for the mean velocity profile, skin-friction coefficient, etc[7]. Compatible model constraints to construct new SGS model is proposed and a new model based on the vortex stretching magnitude is built and is tested in LES of decaying isotropic turbulent flow and turbulent plane-channel flow[8]. A dynamic regularized gradient model of subgrid stress tensor is developed based on a priori tests to improve the accuracy of global SGS dissipation[9]. A new mixed model that better accounts for the physics of the SGS stress and

ing the backscatter is developed. The model provides significant backscatter and remains stable[10]. A subgrid scale velocity and scalar field with a uniform mean scalar gradient are generated using the multi-scale turnover Lagrangian map. The statistics such as SGS energy dissipation, scalar variance dissipation, and scalar variance from the synthetic method are compared with those from the DNS with good accuracy[11]. Owing to the low computational cost, LES has become a truly attractive choice for practical turbulent flow simulations at high Reynolds numbers. However, the strong influence of the missing small-scale turbulent motions on the relative dispersion of the particles represents a long-standing challenge in the LES of particle-laden turbulent flows. According to previous studies, the LES cannot accurately predict the Lagrangian relative dispersion of fluid particles and inertial particles in turbulent flows due to the lack of small-scale motions and SGS model errors[14–21]. An accurate description of the Lagrangian dispersion of fluid particles is essential for describing turbulent mixing and transport processes. Therefore, the SGS model for an accurate prediction of particle statistics is definitely needed to compensate for small-scale velocity fluctuations in the LES of isotropic turbulent flows.

There have been various attempts at developing SGS models for the effects of turbulent flows on the prediction of the Lagrangian dispersion of fluid or inertial particles, including the approximate deconvolution model (ADM)[22–24] for the resolved scales, stochastic model[25,26], kinematic simulation (KS) model[27–29], fractal interpolation method[20,30] and spectrally optimized interpolation method[31] for the unresolved scales. Geurts[22] constructed generalized similarity models based on the approximate polynomial inversion of the top-hat filter and improved the kinetic energy transfer to small scales in the LES. Stolz and Adams[23] developed an ADM for LES, which could approximately deconvolve the dependent variables by a truncated series expansion of the inverse filter. Then, the ADM was applied to obtain an approximation of the unfiltered solution for the LES of different flows, such as turbulent channel flows[24,32], turbulent gas-solid flows[12], particle-laden homogeneous shear turbulent flows[33,34] and isotropic turbulent flows[35,36]. The structural ADM has been used in large-eddy simulation of gas-solid flows described by two-fluid model, and the approach has excellent performance in modeling the drag force and Reynolds-stress of the particle phase[12]. Recently, Park et al.[37] proposed a dynamic model based on elliptical differential filters for the LES of particle-laden turbulent flows to model the SGS velocity and describe the motion of the small inertial particles[38,39]. This model not limited into isotropic flows and is flexible

enough to be used in any type complex configurations and grids. However, the aforementioned ADM can only improve the resolved scales of the turbulence represented on the grid of the LES but cannot contribute to the unresolved scales of the velocity fluctuations.

There are four types of SGS models developed to model the effects of the missing subgrid scales of turbulence on the particle dispersion in the LES. The first type of SGS model is the stochastic model. The lack of the unresolved scales of the velocity fluctuations can be compensated by the solutions of the Langevin equations supplemented with random sources[25,26], which depend on the Wiener processes[40–42]. The temporal evolution of the Lagrangian velocities generated by the stochastic model is similar to Brownian motion with drift. This stochastic model has been typically used to study the turbulent dispersion of single-particle[43,44], two-particle[40,45,46] and four-particle[47,48]. The second type of SGS model is the KS model. Kraichnan generated incompressible, isotropic turbulence using a set of Fourier components[27]. The KS was then used to generate turbulent-like flow structures and calculate the Eulerian or Lagrangian statistics of the isotropic turbulent flows[49–52]. Malik and Vassilicos[53] formulated a direct comparison between the statistical results of the two-particle dispersion from the DNS[54] for statistically stationary isotropic turbulent flows and those from the KS. The good agreement demonstrates that the KS is an accurate Lagrangian model for fluid particle dispersion in isotropic turbulent flows. Afterwards, Flohr and Vassilicos[55] coupled the KS to LES velocity fields and investigated the performance of the KS on two-particle dispersion in isotropic turbulent flows. Ray and Collins[18] applied a modified KS based subgrid model to predict the clustering of inertial particles in the LES of homogeneous and isotropic turbulence. In the third type of SGS model, a fractal interpolation approach was applied as a structural model for subgrid particle dispersion in the LES of turbulent dispersed flows by Marchioli et al.[30]. The fourth type of particle SGS model is a spectrally optimized interpolation method, which was proposed by Gobert and Manhart[31] to account for the SGS velocity fluctuations in Lagrangian particle simulations.

To simultaneously model the effects of the resolved scales and subgrid scales of turbulent motions on particle dispersion, a hybrid stochastic-deconvolution model was developed for the particle motion in the LES of particle-laden turbulent channel flow[56]. The objective of this paper is to develop a kinematic simulation with an approximate deconvolution (KSAD) SGS model for the Lagrangian relative dispersion of fluid particles in the LES of homogeneous and isotropic turbulence. For the resolved scales in the LES, the ADM is applied

approximate the unfiltered solution of the flow field, especially the enstrophy, which is crucial to improve the energy flux or energy dissipation rate used in the KS model. For the subgrid scales, the KS is used to compensate for the missing velocity fluctuations. The improvement of the hybrid model in the prediction of the Lagrangian relative dispersion of fluid particles in the LES of isotropic turbulent flows is evaluated in detail.

The structure of this paper is organized as follows: In Section II, we describe the details of the numerical methods used to resolve the homogeneous and isotropic turbulent flow field and track the fluid particle motion. In Section III, the implementations of the ADM and KS are described in detail. Moreover, we show the recovered energy spectra of isotropic turbulent flows after implementing the models. Section IV discusses the performance of the KS with different input parameters and shows the predictions of the Lagrangian statistics of two- and four-particle dispersion by the KSAD SGS model. Section V gives the conclusions.

II. NUMERICAL METHODS

A. Direct numerical simulation

The Navier-Stokes equations for incompressible flows with constant physical properties are

$$\frac{\partial \mathbf{u}}{\partial t} = \mathbf{u} \times \boldsymbol{\omega} - \nabla \left(\frac{p}{\rho} + \frac{1}{2}\mathbf{u}^2 \right) + \nu \nabla^2 \mathbf{u} + \mathbf{f}\left(\mathbf{x}, t\right), \tag{1}$$

$$\nabla \cdot \mathbf{u} = 0, \tag{2}$$

where $\mathbf{u}$ denotes the velocity field, $\boldsymbol{\omega} = \nabla \times \mathbf{u}$ denotes the vorticity field, p is the pressure, ρ is the fluid density, and ν is the kinematic viscosity. The turbulent flow was driven by a deterministic forcing term $\mathbf{f}\left(\mathbf{x}, t\right)$, which is non-zero for the Fourier modes with a wavenumber magnitude less than or equal to 2. With this deterministic forcing method, a stationary turbulence was generated by maintaining the constant total energy in each of the first two wavenumber shells, and the energy ratio between the two shells was consistent with the $k^{-5/3}$ scaling[57].

The DNS of homogeneous and isotropic turbulent flows was performed using a standard pseudo-spectral method in a periodic cubic flow domain with each edge length $L = 2\pi$, which was discretized uniformly into N^3 grids. In Fourier space, Eqs. (1) and (2) can be

This manuscript was accepted by Phys. Fluids. Click here to see the version of record.

represented as ($k \leq k_{\max}$)

$$\left(\frac{\partial}{\partial t}+\nu k^2\right)\hat{\mathbf{u}}\left(\mathbf{k},t\right)=\mathbf{P}\left(\mathbf{k}\right)\mathcal{F}\left(\mathbf{u}\times\boldsymbol{\omega}\right)+\hat{\mathbf{f}}\left(\mathbf{k},t\right), \tag{3}$$

where $\hat{\mathbf{u}}\left(\mathbf{k},t\right)$ denotes the Fourier coefficient or the fluid velocity in Fourier space and $\mathcal{F}$ denotes the Fourier transformation. The projection tensor $\mathbf{P}\left(\mathbf{k}\right)=\delta_{ij}-k_ik_j/k^2\,(i,j=1,2,3)$ projects $\mathcal{F}\left(\mathbf{u}\times\boldsymbol{\omega}\right)$ onto the plane normal to the wavenumber vector $\mathbf{k}$ and eliminates the pressure gradient term in Eq. (1). The wavenumber components in Fourier space were defined as $k_j=n_j\left(2\pi/L\right)$, where $n_j=-N/2,\ldots,-1,0,1,\ldots,N/2-1$ for $j=1,2,3$. The maximum wavenumber was approximately $N/3$, and $N=512$ was set in the DNS. The spatial resolution was monitored by the value of $k_{\max}\eta$, where η is the Kolmogorov length scale. The value of $k_{\max}\eta$ should be larger than 1.0 for the Kolmogorov scale of the flow to be well resolved, and it was always larger than 1.3 in our simulations. The Fourier coefficients of the flow velocity were advanced in time using a second-order Adams-Bashforth method for the nonlinear term and an exact integration for the linear viscous term. The time step was chosen to ensure that the Courant-Friedrichs-Lewy (CFL) number is 0.5 or less for numerical stability and accuracy.

B. Large eddy simulation

The LES of homogeneous and isotropic turbulent flows was performed at a much coarser grid resolution using the same pseudo-spectral method and large-scale forcing scheme as the above DNS. The governing equation for the LES is given by

$$\left(\frac{\partial}{\partial t}+\left[\nu+\nu_e\left(k\,|k_c\right)\right]k^2\right)\hat{\bar{\mathbf{u}}}\left(\mathbf{k},t\right)=\mathbf{P}\left(\mathbf{k}\right)\mathcal{F}\left(\bar{\mathbf{u}}\times\bar{\boldsymbol{\omega}}\right)+\hat{\mathbf{f}}\left(\mathbf{k},t\right), \tag{4}$$

where $\bar{\mathbf{u}}$ and $\bar{\boldsymbol{\omega}}$ are the resolved velocity and vorticity in physical space, respectively. A spectral eddy-viscosity SGS model is used[58,59],

$$\nu_e\left(k\,|k_c\right)=\nu_e^{+}\left(k\,|k_c\right)\sqrt{E\left(k_c\right)/k_c}, \tag{5}$$

$$\nu_e^{+}\left(k\,|k_c\right)=C_k^{-3/2}\left[0.441+15.2\exp\left(-3.03\,k_c/k\right)\right]. \tag{6}$$

Here, $\nu_e\left(k\,|k_c\right)$ denotes the spectral eddy-viscosity and k_c denotes the cutoff wavenumber in the LES. The quantity $E\left(k_c\right)$ is the value of energy spectrum at the cutoff wavenumber, which is instantaneously evaluated from the LES, and $C_k=2.0$ was used in this work. The

above SGS model was constructed based on the turbulent energy budget equations, which basically predicted the energy spectrum, especially at low wavenumbers. The hypothesis of a $k^{-5/3}$ energy spectrum up to k_c was used to parameterize the SGS model. This hypothesis is believed to be better fulfilled in turbulent flows with increasing Reynolds numbers.

C. Filtered direct numerical simulation

The velocity field of the filtered direct numerical simulation (FDNS) was obtained from the DNS velocity field by truncating the Fourier coefficients larger than the cutoff wavenumber k_c with a sharp spectral filter

$$\tilde{\boldsymbol{u}}(\mathbf{x},t)=\sum_{|\mathbf{k}|=k_0}^{k_c}\hat{\mathbf{u}}(\mathbf{k},t)\,e^{i\mathbf{k}\cdot\mathbf{x}}, \tag{7}$$

where $\tilde{\boldsymbol{u}}(\mathbf{x},t)$ is the filtered velocity in physical space and $k_0=1$ denotes the lowest wavenumber in the DNS. The Eulerian statistics of flow fields from the DNS, FDNS and LES are listed in Table I. In the isotropic turbulent flows with zero mean velocity, the Taylor Reynolds number Re_λ is defined as

$$Re_\lambda=u'\lambda/\nu, \tag{8}$$

where $u'=\sqrt{\langle u_iu_i\rangle/3}$ is the root mean square (rms) of turbulent fluctuating velocity, $\lambda=\left(15\nu u'^2/\varepsilon\right)^{1/2}$ is the Taylor microscale. For the setting of DNS 512^3, two cases of LES are performed with the closure of the eddy-viscosity model: the first uses 64^3 grid resolution and the second uses 32^3 grid resolution. For the FDNS, the cutoff wavenumber is $k_c=42$.

D. Fluid particle motion

For a fluid particle in isotropic turbulent flows, the equation of motion is

$$\frac{\partial\mathbf{X}(\mathbf{x}_0,t_0\,|t)}{\partial t}=\mathbf{V}(\mathbf{x}_0,t_0\,|t)=\mathbf{u}\left[\mathbf{X}(\mathbf{x}_0,t_0\,|t),t\right], \tag{9}$$

where $\mathbf{X}(\mathbf{x}_0,t_0\,|t)$ is the location of the fluid particle at time t, which was initially located at $\mathbf{x}_0$ and time t_0, and $\mathbf{V}(\mathbf{x}_0,t_0\,|t)$ is the Lagrangian velocity of the fluid particle at time t, which is equal to the Eulerian velocity $\mathbf{u}\left[\mathbf{X}(\mathbf{x}_0,t_0\,|t),t\right]$ of the flow field at location $\mathbf{X}(\mathbf{x}_0,t_0\,|t)$.

TABLE I. Eulerian statistics of flow fields from different cases.

Case	DNS	FDNS	LES	LES
Grid Number N^3	512^3	—	64^3	32^3
Maximum wavenumber k_{max} (k_c)	170	42	21	10
Grid length dx	0.012	—	0.098	0.196
Kinematic viscosity ν	0.0010	0.0010	0.0010	0.0010
Taylor Reynolds number Re_λ	205.51	—	—	—
rms fluctuating velocity u'	0.870	0.866	0.854	0.819
Dissipation rate ε	0.204	—	—	—
Spatial resolution $k_{max}\eta$	1.432	—	—	—
Kolmogorov length scale η	0.00835	—	—	—
Kolmogorov time scale τ_η	0.06976	—	—	—

A three-dimensional sixth-order Lagrangian interpolation scheme was used to calculate the Lagrangian velocity of the fluid particle from the Eulerian flow velocity field. Then, the trajectory of the fluid particle was obtained by the explicit fourth-order Adams-Bashforth scheme. To completely demonstrate the statistical properties of the fluid particles, we tracked the motion of an ensemble of particle pairs and clusters of four particles and calculated the various Lagrangian statistics. Initially, $N_p/4$ particles are uniformly distributed in the flow domain. The other $3N_p/4$ particles are located under the constraint that each of the four particles form a tetrahedron with a prescribed edge size. Thus, the $N_p/4$ regular tetrahedrons with initially prescribed edge sizes are randomly distributed, and each tetrahedron consists of six particle pairs with a prescribed separation distance. The Lagrangian statistics were calculated from ensemble averaging, including space averaging and time averaging. Here, the time averaging denotes the average of the independent samples of Lagrangian statistics from the different time segments.

This manuscript was accepted by Phys. Fluids. Click here to see the version of record.

III. HYBRID MODEL

A. Approximate deconvolution model

There are two main reasons for the errors in the flow field in the LES compared to the DNS. One reason is the filtering operation on the Navier-Stokes equations, which leads to the loss of SGS velocity fluctuations. The other reason is the spectral eddy-viscosity SGS model used in this paper, which has a strong hyperviscosity near the cutoff wavenumber. The model causes over-dissipation of turbulent energy and a further reduction in the velocity fluctuations at the resolved scales, especially at the scale of the cutoff wavenumber. To approximate the unfiltered solution of the flow field at resolved scales, we applied an ADM to the filtered velocity field in the LES,

$$\hat{\mathbf{u}}^* = \hat{G}^{-1}\hat{\bar{\mathbf{u}}}, \tag{10}$$

where $\hat{\bar{\mathbf{u}}}$ is the filtered velocity of LES, $\hat{\mathbf{u}}^*$ is an approximation of the unfiltered velocity, and $\hat{G}$ is a filter function in spectral space, and

$$\hat{G}^{-1}(k) \approx \sum_{n=0}^{N} \left(1 - \hat{G}(k)\right)^n. \tag{11}$$

According to the study of Stolz and Adams[23], $N = 5$ provides proper results for most of the cases studied, so that

$$\hat{G}^{-1}(k) \approx 6 - 15\hat{G}(k) + 20\hat{G}^2(k) - 15\hat{G}^3(k) + 6\hat{G}^4(k) - \hat{G}^5(k). \tag{12}$$

The filter $\hat{G}(k)$ must satisfy $\left|1 - \hat{G}(k)\right| < 1$ and have an inversion. Substituting Eq. (12) into Eq. (10), the velocity $\hat{\mathbf{u}}^*$ can be calculated by the repeated filtering of $\hat{\bar{\mathbf{u}}}$

$$\hat{\mathbf{u}}^* \approx 6\hat{\bar{\mathbf{u}}} - 15\hat{\bar{\bar{\mathbf{u}}}} + 20\hat{\bar{\bar{\bar{\mathbf{u}}}}} - 15\hat{\bar{\bar{\bar{\bar{\mathbf{u}}}}}} + 6\hat{\bar{\bar{\bar{\bar{\bar{\mathbf{u}}}}}}} - \hat{\bar{\bar{\bar{\bar{\bar{\bar{\mathbf{u}}}}}}}}. \tag{13}$$

In this work, we chose a three-dimensional transfer function of Gaussian

$$\hat{G}(k) = \exp\left(-\frac{|\mathbf{k}^2|\,\Delta^2}{24}\right), \quad \Delta = \pi/k_c. \tag{14}$$

For Gaussian transfer function, Eq. (14) and $N = 5$, the inverse of the transfer function $\hat{G}^{-1}(k)$ in LES 64^3 is shown in Fig. 1. It shows the approximate inverse function is always

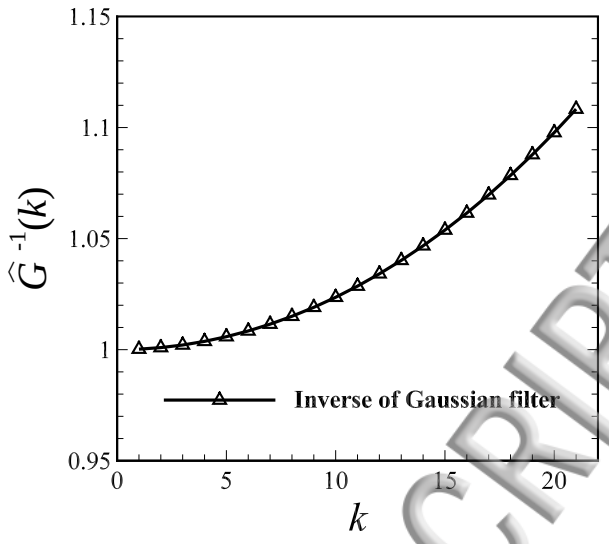

FIG. 1. The approximate inverse transfer function of Gaussian using Eq. (12) in LES 64^3.

greater than 1.0 and increases with the wavenumber. Thus the approximate inverse transfer function can strength the motions at smaller scales.

Fig. 2 shows the energy and dissipation spectra obtained from the DNS, LES and LES with the ADM. The ADM recovers the energy and dissipation spectra near the cutoff wavenumber in the LES. The small-scale velocities near the cutoff wavenumber are significantly improved. Notably, the last point in the dissipation spectrum is over-corrected by the ADM, which comes from the unphysical accumulation of energy near the cutoff wavenumber[19]. The unphysical accumulation in the energy spectrum is amplified in the dissipation spectrum.

B. Kinematic simulation

To compensate for the velocity fluctuations at the subgrid scales, we used a KS model to calculate the subgrid velocity[18]. The standard form of the KS velocity field is

$$\mathbf{u}_{\mathrm{KS}}(\mathbf{x},t)=\sum_{n=1}^{N_k}\sum_{m=1}^{M}\left\{\mathbf{a}_{nm}\cos\left(\mathbf{k}_{nm}\cdot\mathbf{x}+\omega_{nm}t\right)+\mathbf{b}_{nm}\sin\left(\mathbf{k}_{nm}\cdot\mathbf{x}+\omega_{nm}t\right)\right\}, \tag{15}$$

where $\mathbf{a}_{nm}$ and $\mathbf{b}_{nm}$ are the vector coefficients of the Fourier cosine and sine modes of the velocity, respectively, $\mathbf{k}_{nm}$ is the wavevector, $\mathbf{x}$ is the coordinate vector, ω_{nm} is the frequency and t is the time. The indices 'nm' are used in a spherical coordinate system, where 'n' denotes the magnitude of the wavenumber $k_n=|\mathbf{k}_{nm}|$ and 'm' is the counter of randomly

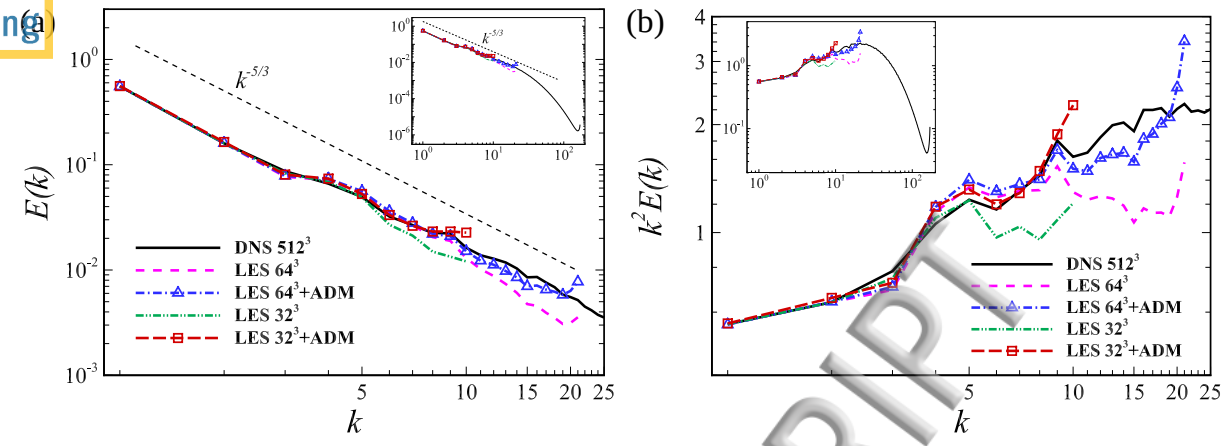

FIG. 2. (a) Energy and (b) dissipation spectra for the DNS 512^3, LES 64^3 and 32^3, and LES with the ADM.

oriented wavevectors of magnitude k_n. To achieve the fastest convergence for fluid particle statistics, we used a geometric distribution of wavenumbers beyond the cutoff wavenumber[55]

$$k_n = k_c \left(\frac{k_{\max}}{k_c} \right)^{\frac{n-1}{N_k-1}}, \tag{16}$$

$$\mathbf{k}_{nm} = k_n \left(\sin\theta_{nm} \cos\phi_{nm}, \sin\theta_{nm} \sin\phi_{nm}, \cos\theta_{nm} \right), \tag{17}$$

where $n = 1, 2, \ldots, N_k$ and $k_{\max}$ is the largest wavenumber considered. The orientation angles θ_{nm} and ϕ_{nm} for the M wavevectors associated with each wavenumber were chosen randomly to be uniformly distributed over the spherical shell of radius k_n

$$\cos\theta_{nm} \in [-1, 1], \qquad \phi_{nm} \in [0, 2\pi]. \tag{18}$$

To ensure the incompressibility of the subgrid velocity $\mathbf{u}_{\mathrm{KS}}(\mathbf{x}, t)$, we define the coefficients $\mathbf{a}_{nm}$ and $\mathbf{b}_{nm}$ as

$$\mathbf{a}_{nm} = \mathbf{A}_{nm} \times \hat{\mathbf{k}}_{nm}, \tag{19}$$

$$\mathbf{b}_{nm} = \mathbf{B}_{nm} \times \hat{\mathbf{k}}_{nm}, \tag{20}$$

where $\hat{\mathbf{k}}_{nm} = \mathbf{k}_{nm}/k_n$ is a unit vector aligned with the wavevector $\mathbf{k}_{nm}$. $\mathbf{A}_{nm}$ and $\mathbf{B}_{nm}$ are random vectors with independent and normally distributed components, each with a mean of zero and a variance of σ_n^2

$$\sigma_n^2 = \frac{1}{M} E(k_n) \Delta k_n, \tag{21}$$

where $\Delta k_n = (k_{n+1} - k_{n-1})/2$ for $n \in [2, N_k - 1]$, $\Delta k_1 = (k_2 - k_1)/2$, and $\Delta k_{N_k} = (k_{N_k} - k_{N_k-1})/2$. $E(k_n)$ denotes the subgrid energy spectrum at k_n, which can be approximated by the DNS spectrum or a known model spectrum[60]

$$E(k) = C_k \varepsilon^{2/3} k^{-5/3} f_\eta(k\eta), \tag{22}$$

$$f_\eta(k\eta) = \exp\left\{-\beta\left\{\left[(k\eta)^4 + c_\eta^4\right]^{1/4} - c_\eta\right\}\right\}, \tag{23}$$

where the dissipation rate $\varepsilon = \int_0^{k_{\max}} 2(\nu + \nu_e) k^2 E(k)\,\mathrm{d}k$ and the Kolmogorov length scale $\eta = (\nu^3/\varepsilon)^{1/4}$ can be calculated from the LES flow field after using the ADM. Additionally, $C_k = 2.0$, $\beta = 5.2$, and $c_\eta \approx 0.25$.

The frequency ω_{nm} determines the unsteadiness associated with the wave mode n and is usually chosen to be proportional to the eddy-turnover time of the wave mode n

$$\omega_{nm} = \lambda\sqrt{k_{nm}^3 E(k_{nm})}, \tag{24}$$

where λ is a dimensionless constant of order 1. Previous studies have shown that the temporal term $\omega_{nm}t$ has little effect on the statistics of the fluid particle pairs[53], which is also validated in our simulations. Therefore, we set $\omega_{nm} = 0$ in the KS, so that the velocity field was essentially frozen at all scales.

After constructing the incompressible subgrid velocity field $\mathbf{u}_{\mathrm{KS}}(\mathbf{x}, t)$, the modeled velocity field at each particle position could be written as

$$\mathbf{u}_{\mathrm{MODEL}}(\mathbf{x}, t) = \mathbf{u}_{\mathrm{LES/FDNS}}(\mathbf{x}, t) + \mathbf{u}_{\mathrm{KS}}(\mathbf{x}, t), \tag{25}$$

where $\mathbf{u}_{\mathrm{LES/FDNS}}(\mathbf{x}, t)$ is the particle velocity calculated from the LES or FDNS flow field.

By using the KS, we obtained the subgrid velocity at each location of the flow field with 512^3 grids, which was used to compensate for the FDNS velocity field. The cutoff wavenumber is $k_c = 42$, and the maximum wavenumber is $k_{\max} = 170$. To minimize modeling errors, we used the energy spectrum of DNS 512^3 as the input parameters in the a priori LES or FDNS

$$E(k_c)|_{\mathrm{KS}} = E(k_c)|_{\mathrm{FDNS}}. \tag{26}$$

In the a posteriori LES, we used the corrected energy spectrum with the ADM

$$E(k_c)|_{\mathrm{KS}} = E(k_c)|_{\mathrm{LES+ADM}}. \tag{27}$$

Eqs. (26) and (27) establish the relationship between the SGS flow field and the LES flow field.

The number of wavenumbers were varied from 50 ($N_k = 50$, $M = 1$) to 10000 ($N_k = 200$, $M = 50$), and the comparisons of the energy spectra obtained from the DNS and the FDNS plus KS with different $N_k \times M$ are shown as Fig. 3. It is observed that the KS recovers the missing subgrid energy spectrum at $k \geq k_c$ quite accurately when $N_k \geq 150$ and $M \geq 20$. Otherwise, the computed subgrid energy spectrum will fluctuate around the input DNS energy spectrum.

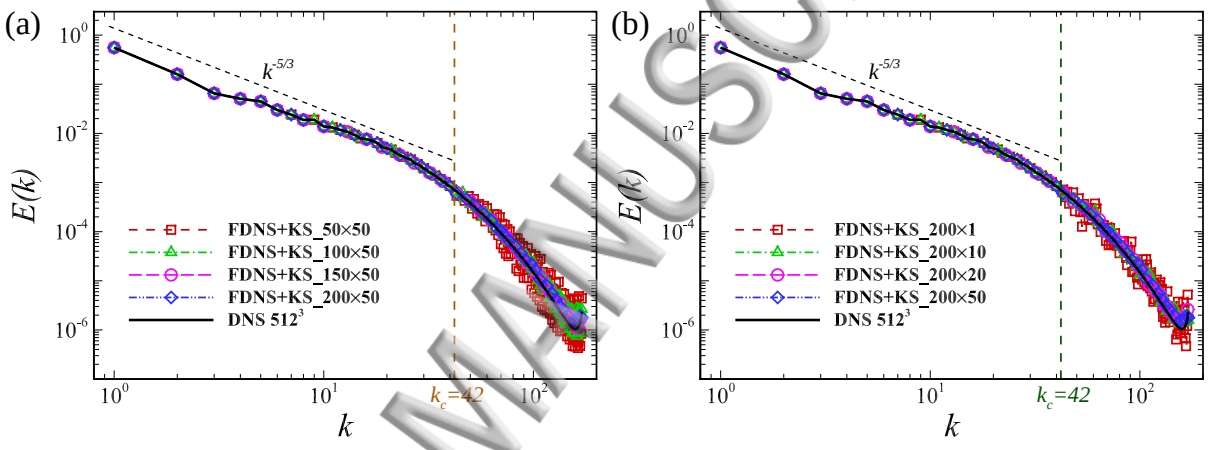

FIG. 3. Comparison of the energy spectra obtained from the DNS 512^3 and FDNS plus KS with a cutoff wavenumber, $k_c = 42$. The KS nearly recovers the subgrid energy spectrum beyond k_c.

IV. RESULTS AND DISCUSSION

In this work, we set $N_p = 50000$, and fluid particles were divided into five groups, in which the initial separation distances were $r = 1/4\eta$, 1η, 8η, 32η, and 96η. After tracking the trajectory of each fluid particle, we calculated the Lagrangian statistics of single-, two- and four-particle dispersion in the DNS, LES and LES plus KSAD hybrid model. Then, we compared the Lagrangian statistics calculated from the LES plus KSAD hybrid model with the results from the DNS and LES and evaluated the availability of the model.

This manuscript was accepted by Phys. Fluids. Click here to see the version of record.

Ag Parametric study for KS

The total number of wavevectors in the KS is important for predicting the Lagrangian dispersion of fluid particles because it determines both the modeling accuracy and computational cost. To investigate the effect of the number of wavevectors on the prediction of the fluid particle statistics, we set $N_k \times M$ as 20×1, 50×50 and 200×20. Here, we used the DNS spectrum to approximate the input subgrid energy spectrum in Eq. (21).

For the particle pair shown as Fig. 4, the separation distance is defined as

$$R\left(\mathbf{r}, t_0 \left| \tau \right.\right) = \sqrt{\mathbf{R}\left(\mathbf{r}, t_0 \left| \tau \right.\right) \cdot \mathbf{R}\left(\mathbf{r}, t_0 \left| \tau \right.\right)}, \tag{28}$$

$$\mathbf{R}\left(\mathbf{r}, t_0 \left| \tau \right.\right) = \mathbf{X}\left(\mathbf{x}_0, t_0 \left| t_0 + \tau \right.\right) - \mathbf{X}\left(\mathbf{x}_0 + \mathbf{r}, t_0 \left| t_0 + \tau \right.\right), \tag{29}$$

where $\mathbf{R}\left(\mathbf{r}, t_0 \left| \tau \right.\right)$ denotes the separation vector between the particle pair, $\mathbf{r}$ is the initial separation vector and τ is the time interval. The initial separation of the particle pair shown in Fig. 4 is very small, and it seems like they collapse together. With increasing time, the particles separate. Then, the mean and variance of the separation distance were calculated

$$m_2\left(r, \tau\right) = \left\langle R\left(\mathbf{r}, t_0 \left| \tau \right.\right) \right\rangle, \tag{30}$$

$$\sigma_2^2\left(r, \tau\right) = \left\langle \left[R\left(\mathbf{r}, t_0 \left| \tau \right.\right) - \left\langle R\left(\mathbf{r}, t_0 \left| \tau \right.\right) \right\rangle \right]^2 \right\rangle = \left\langle \mathbf{R}\left(\mathbf{r}, t_0 \left| \tau \right.\right) \cdot \mathbf{R}\left(\mathbf{r}, t_0 \left| \tau \right.\right) \right\rangle - m_2^2\left(r, \tau\right), \tag{31}$$

where $\langle\ \rangle$ denotes the ensemble average conditioned on the particle pairs, and $r = |\mathbf{r}|$ denotes the initially prescribed separation distance. Then, the relative dispersion of the particle pair is defined as $\left\langle \delta\mathbf{R}\left(r, \tau\right) \cdot \delta\mathbf{R}\left(r, \tau\right) \right\rangle$, where $\delta\mathbf{R}\left(r, \tau\right) = \mathbf{R}\left(\mathbf{r}, t_0 \left| \tau \right.\right) - \mathbf{r}$ is the separation vector increment.

The one-time two-point Lagrangian velocity correlation function of the particle pair is defined as

$$\rho_r\left(r, \tau\right) = \left\langle V_i\left(\mathbf{x}_0, t_0 \left| t_0 + \tau \right.\right) V_i\left(\mathbf{x}_0 + \mathbf{r}, t_0 \left| t_0 + \tau \right.\right) \right\rangle / \sigma_V^2. \tag{32}$$

Fig. 5 shows the abovementioned Lagrangian statistics of the particle pairs obtained from the LES 64^3 plus KS with different numbers of wavevectors. The parameter τ_η denotes the Kolmogorov time scale. For clarity, we only plotted the results from the fluid particles with initial separation distances $r = 1/4\eta$ and 8η. We can observe that the Lagrangian statistics from the LES 64^3 plus KS with 20×1, 50×50 and 200×20 wavevectors coincide well with each other, and all of them show impressive improvements compared with the results from

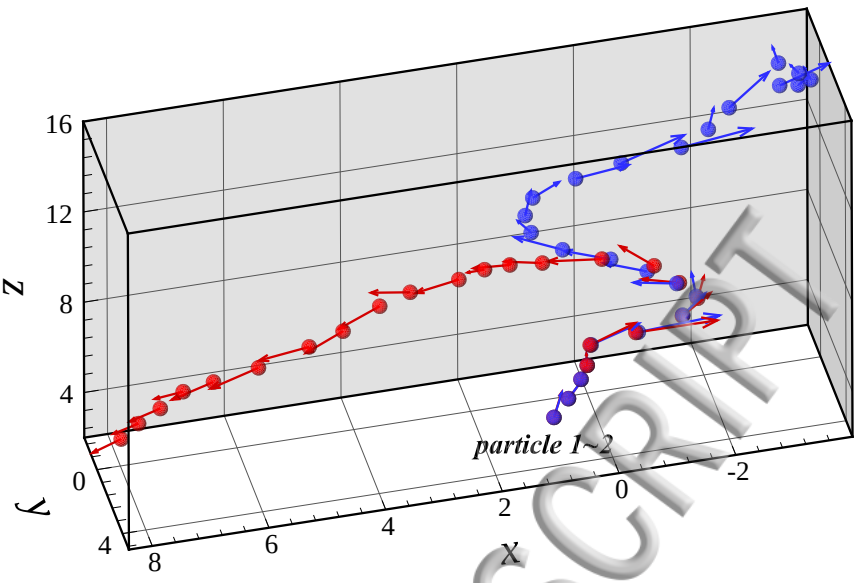

FIG. 4. The schematic diagram of the Lagrangian dispersion of a fluid particle pair with a small initial separation distance in the LES of isotropic turbulent flows. The arrows denote the directions of particle motion.

LES. In addition, a comparison of the Lagrangian statistics of the four-particle dispersion calculated from the LES 64^3 plus KS with different numbers of wavevectors also exhibits great consistency. These results indicate that a more accurate prediction of the Lagrangian dispersion of fluid particles can be achieved by using the KS at a low computational cost.

B. Prediction of the particle-pair dispersion by the KSAD hybrid model

In most practical simulations, we do not have DNS data. Instead, we used the simple model energy spectrum in Eq. (22) as the input energy spectrum and calculated the KS velocity along with each fluid particle, which was then added to the particle velocity obtained from the LES plus ADM. Here, notably, the ADM is very important for the estimation of ε and η in Eq. (22).

To reduce the computational cost of the LES plus KSAD hybrid model, we chose $N_k = 20$, $M = 1$ for the LES 64^3 and $N_k = 40$, $M = 1$ for the LES 32^3. The parameter settings render the KS an economical model compared with the cost of performing an LES. Then, we investigated the contribution of the KSAD hybrid model to the Lagrangian statistics of fluid particles in isotropic turbulent flows as follows.

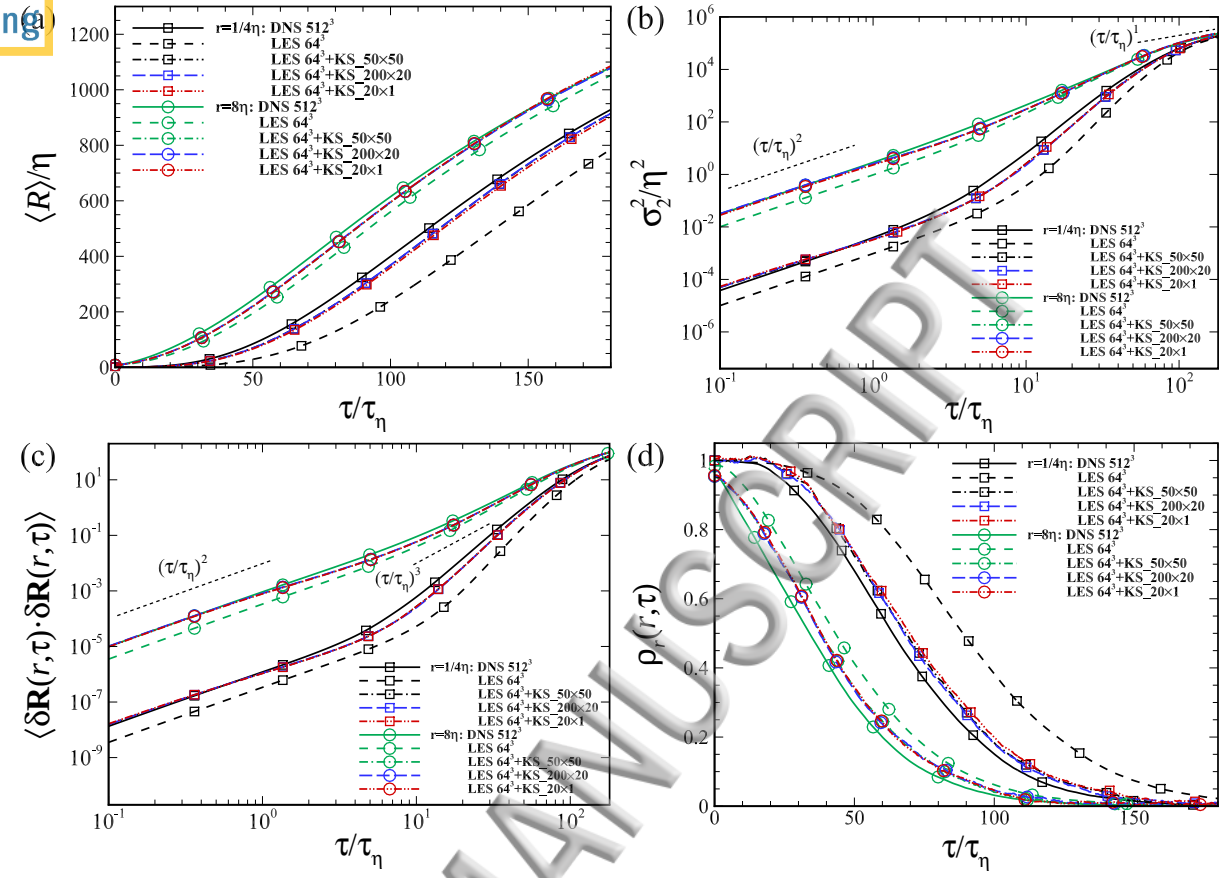

FIG. 5. (a) The mean of the separation distances, (b) the variance of the separation distances, (c) the relative dispersion and (d) the one-time two-point Lagrangian velocity correlation functions of the particle pairs obtained from the LES 64^3 plus KS with different numbers of wavevectors ($N_k \times M$): dash-dotted lines 50×50, long-dashed lines 200×20 and dash-dot-dotted lines 20×1. The symbols '□' and '◯' denote the results of the initial separation distance $r = 1/4\eta$ and 8η, respectively.

Figs. 6 and 7 show the mean and variance of the separation distances of the particle pairs with initial separation distances $r/\eta = 1/4$ and 8. The solid lines, dashed lines, dash-dotted lines, long-dashed lines and dash-dot-dotted lines denote the results obtained from the DNS 512^3, conventional LES and LES with the ADM, KS or KSAD hybrid model, respectively. The LES significantly underpredicts the mean and variance of the separation distances compared to the DNS due to the absence of the small-scale velocity fluctuations. After using the KSAD hybrid model, the deviations of mean separation distances between the LES and DNS are mostly recovered for the particle pairs with small initial separation distances.

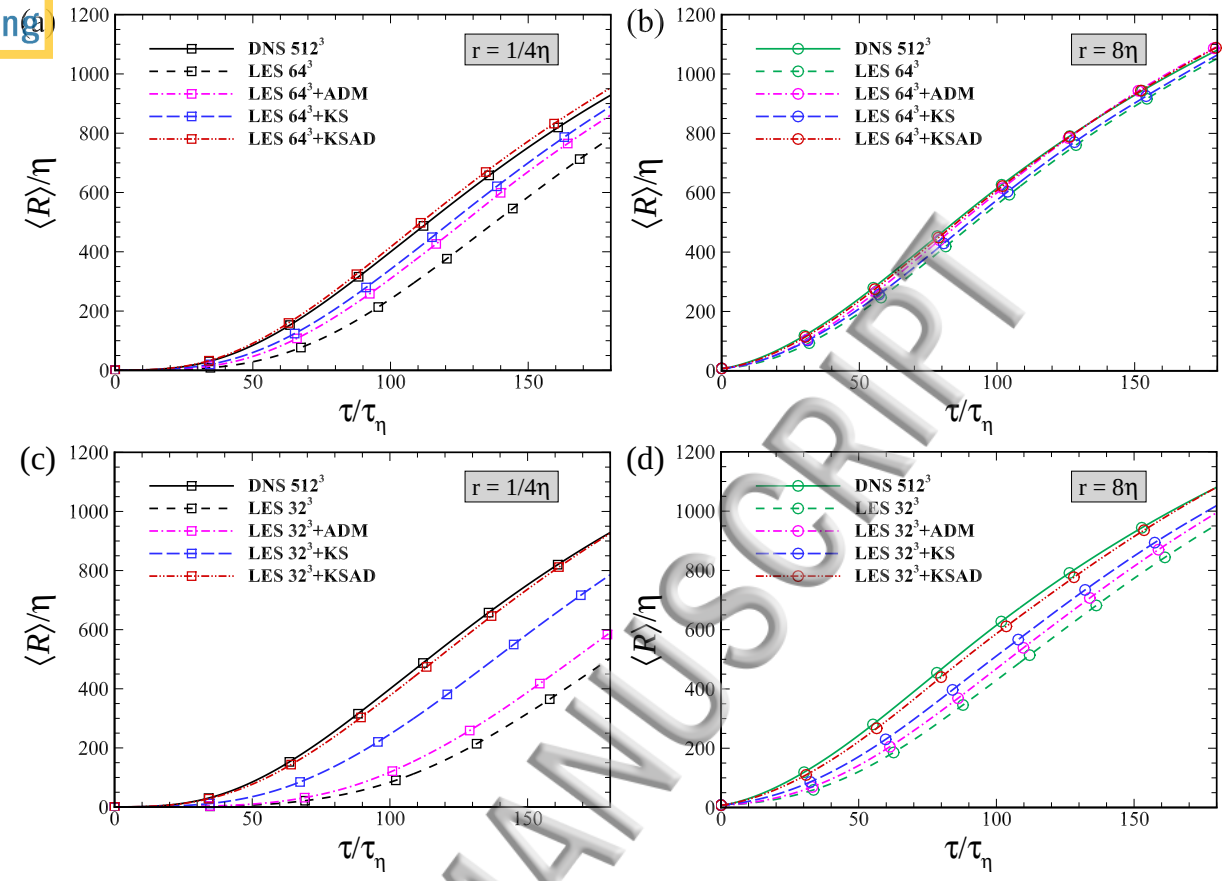

FIG. 6. Temporal evolution of the mean separation distances of the particle pairs with different initial separation distances: solid lines, DNS 512^3; dashed lines, LES; dash-dotted lines, LES with the ADM; long-dashed lines, LES with the KS; and dash-dot-dotted lines, LES with the KSAD hybrid model.

When the initial separation distance becomes larger, the dispersion of particle pairs is mainly controlled by the large-scale motion of the turbulent flows so that the mean separation distances from the different simulations tend to coincide with each other. Moreover, the results calculated from the LES plus KSAD hybrid model agree with those from the DNS 512^3, as shown in Fig. 7, which demonstrate that the subgrid velocity fluctuations of isotropic turbulent flows are successfully recovered.

If only the ADM or KS is applied, then all the Lagrangian statistics are not well predicted. The ADM could both improve the velocity fluctuations at the resolved scales and help construct a better KS at the subgrid scales. Without the ADM, a much smaller dissipation ε and a larger Kolmogorov length scale η in Eq. (22) are calculated from the conventional

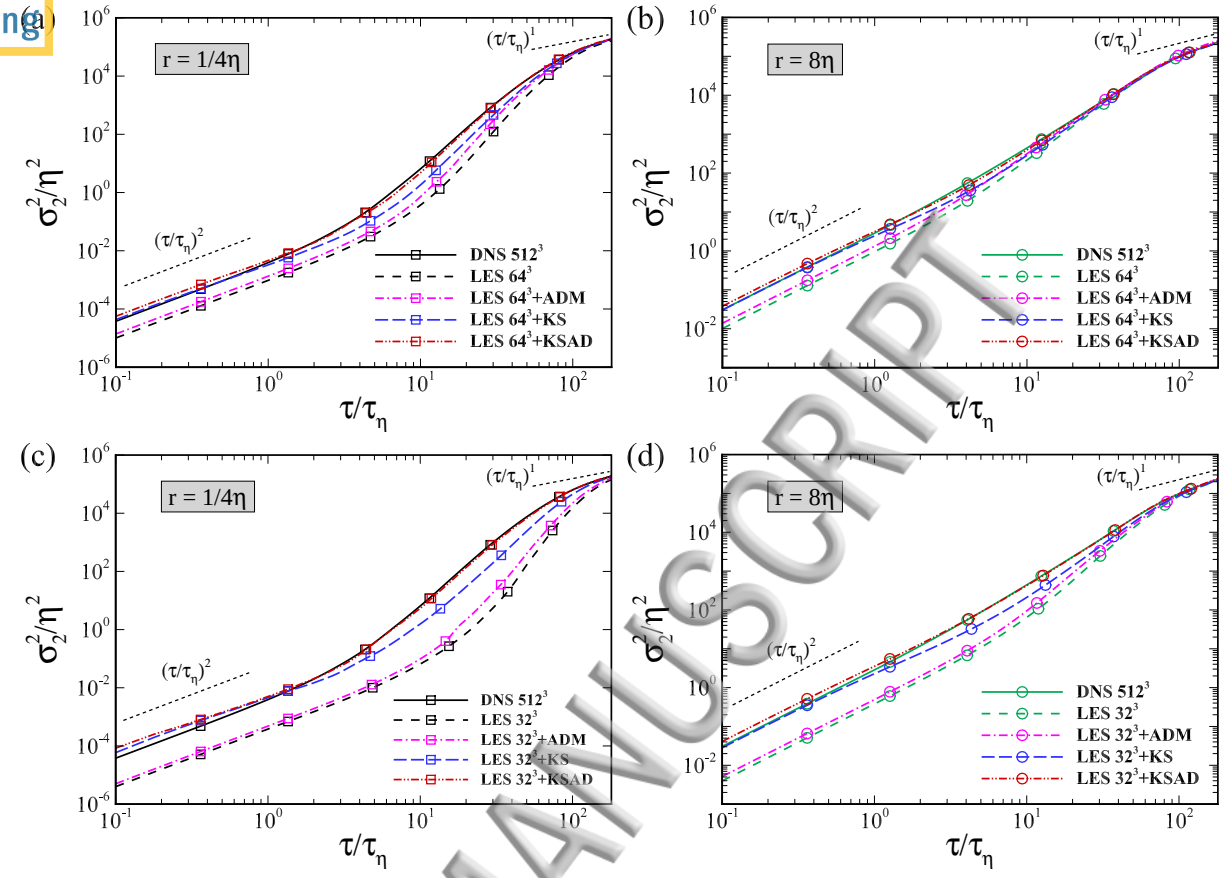

FIG. 7. Temporal evolution of the variances in the separation distances of the particle pairs with different initial separation distances: solid lines, DNS 512^3; dashed lines, LES; dash-dotted lines, LES with the ADM; long-dashed lines, LES with the KS; and dash-dot-dotted lines, LES with the KSAD hybrid model. The left dashed straight line has a slope of 2 and the right top line has a slope of 1.

LES flow field, which result in an underestimation of the model energy and dissipation spectrum, as shown in Fig. 8. Therefore, the mean and variance of the separation distances calculated from the LES plus KS are underpredicted compared with those from the LES plus KSAD hybrid model shown in Figs. 6 and 7. Without the KS, there is only a slight improvement on those Lagrangian statistics by the LES plus ADM for the lack of subgrid velocity fluctuations.

Fig. 9 shows plots of the temporal evolutions of the relative dispersion of particle pairs from the DNS 512^3, LES and LES with the ADM, KS or KSAD hybrid model. One can observe that the LES underpredicts the relative dispersion due to the missing fluctuating

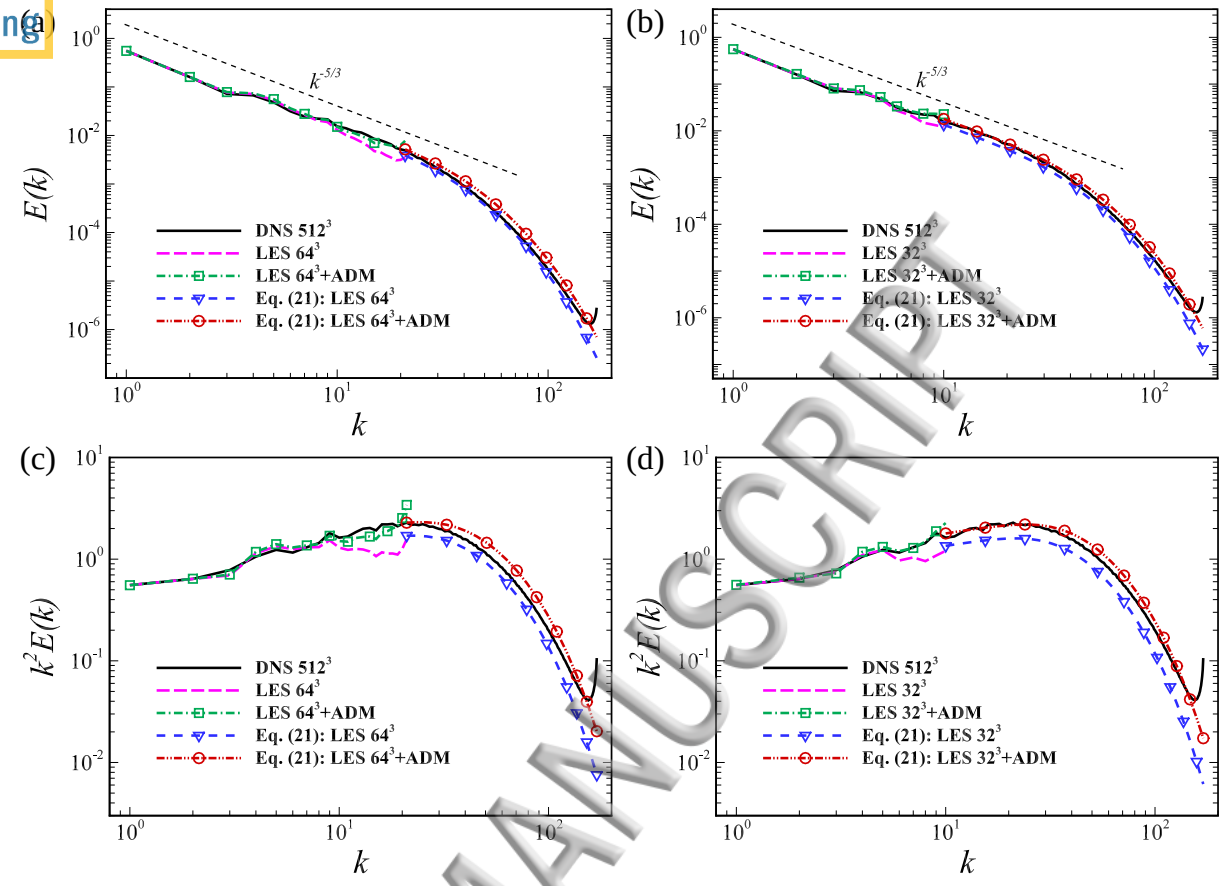

FIG. 8. The comparisons of (a), (b) the input model energy spectra and (c), (d) the input dissipation spectra calculated by Eq. (22) for the LES and LES with the ADM. The dash-dot-dotted lines with symbol '◯' and the dashed lines with symbol '▽' denote the input results from the LES with and without the ADM, respectively.

small-scale fluid motions and SGS model errors. The KSAD hybrid model reproduces the well-defined SGS flow structures and improves the particle dispersion at the beginning. The consistency between the results from the LES plus KSAD hybrid model and DNS show that the hybrid model improves the prediction of the relative dispersion of the particle pairs. Without the ADM, the relative dispersion of the particle pairs is obviously slower because of the underestimation of the KS velocity.

The velocity field in the LES is much more correlated than that in the DNS due to the missing small-scale velocity fluctuations. Therefore, the relative dispersion of the particle pairs in the LES is much slower than that in the DNS. Thus, the one-time two-point Lagrangian velocity correlation functions of the particle pairs in the LES (denoted by dashed

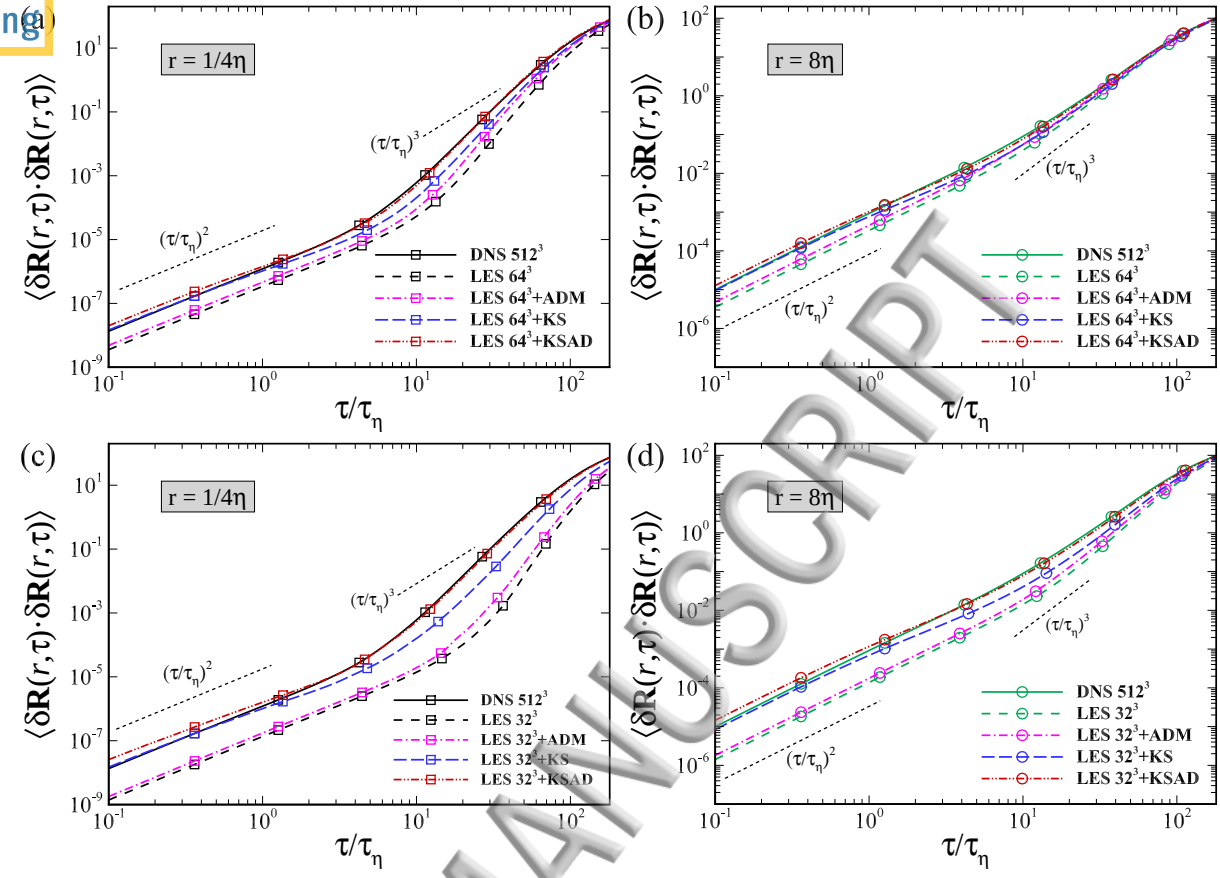

FIG. 9. Temporal evolution of the relative dispersion of the particle pairs with different initial separation distances: solid lines, DNS 512^3; dashed lines, LES; dash-dotted lines, LES with the ADM; long-dashed lines, LES with the KS; and dash-dot-dotted lines, LES with the KSAD hybrid model. The slopes of the left and right dashed lines are equal to 2 and 3, respectively.

lines) decay much slower than those in the DNS 512^3 (denoted by solid lines), as shown in Fig. 10. However, the ADM could improve the kinetic energy near the cutoff wavenumber, and the KS could recover the small-scale velocity fluctuations at unresolved scales. Both models render a more uncorrelated flow field. Therefore, the LES plus KSAD hybrid model, denoted by the long-dashed line, accurately predicts the one-time two-point Lagrangian velocity correlation functions of the particle pairs. With an increase in the initial separation distance, the KS is gradually of no consequence to the Lagrangian statistics of the particle pairs since the large-scale motions of the turbulence dominate the dispersion of the particle pairs.

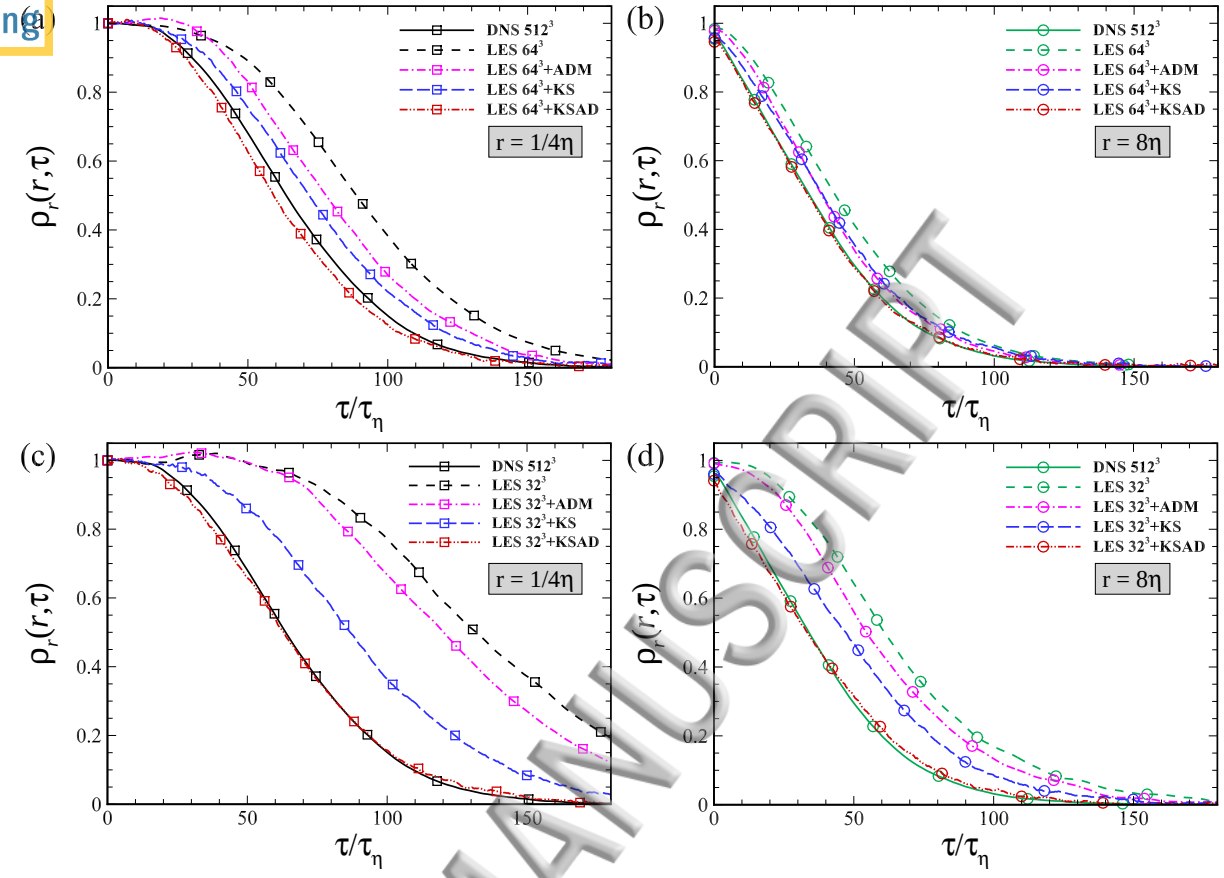

FIG. 10. The one-time two-point Lagrangian velocity correlation functions of the particle pairs with different initial separation distances: solid lines, DNS 512^3; dashed lines, LES; dash-dotted lines, LES with the ADM; long-dashed lines, LES with the KS; and dash-dot-dotted lines, LES with the KSAD hybrid model.

C. Prediction of the four-particle dispersion by the KSAD hybrid model

Multi-particle dispersion provides more information regarding the turbulent transport processes than single- and two-particle dispersion. Here, we focus on the temporal evolution of 2500 tetrahedrons, each formed by four fluid particles. Each edge size of the tetrahedrons is initially set to be equal to the Kolmogorov length scale η. Then, the size and shape of the tetrahedrons change due to the vortex stretching and the small-scale intermittency in isotropic turbulent flows, as shown in Fig. 11. In this section, our purpose is to investigate the effect of the KSAD hybrid model on the prediction of the Lagrangian statistics of four-particle dispersion, including the mean surface area and volume of the tetrahedrons, and their renormalized ratios.

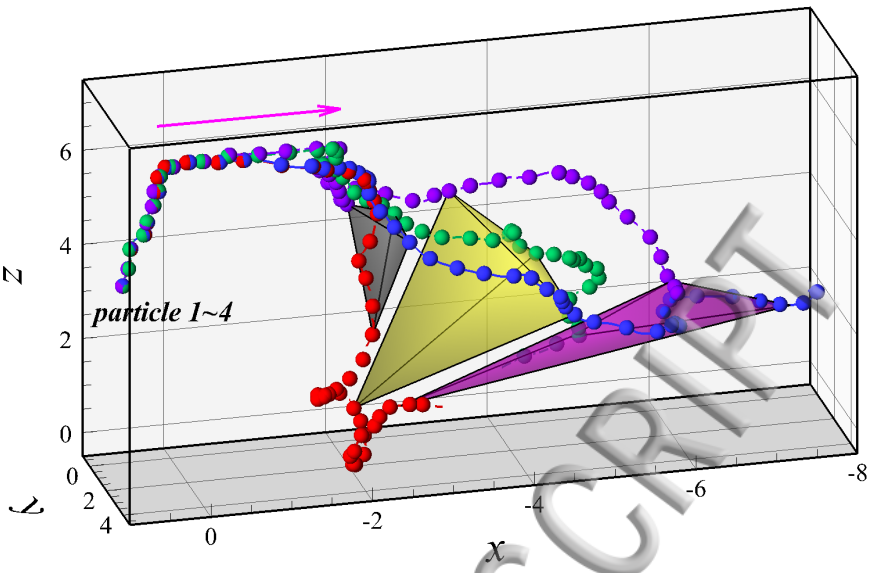

FIG. 11. The schematic diagram of a four-particle dispersion in the LES of isotropic turbulent flows. The four fluid particles form a tetrahedron with a prescribed initial edge size. The size and shape of the tetrahedron change with time. The arrow denotes the direction of the particle motion with an increasing time.

For a regular tetrahedron, the first particle is randomly seeded at $\mathbf{X}_0^{(1)} = (x_0, y_0, z_0)$, and the initial locations of other three particles are $\mathbf{X}_0^{(2)} = \left(x_0 - \sqrt{3}\eta/6, y_0 - \eta/2, z_0 - \sqrt{6}\eta/3\right)$, $\mathbf{X}_0^{(3)} = \left(x_0 - \sqrt{3}\eta/6, y_0 + \eta/2, z_0 - \sqrt{6}\eta/3\right)$ and $\mathbf{X}_0^{(4)} = \left(x_0 + \sqrt{3}\eta/3,\ y_0,\ z_0 - \sqrt{6}\eta/3\right)$. The area of the triangle formed by the first three particles can be calculated by

$$\begin{aligned} S^{(123)} = \frac{1}{2}\Big\{ &\left[\left(y^{(2)} - y^{(1)}\right)\left(z^{(3)} - z^{(1)}\right) - \left(z^{(2)} - z^{(1)}\right)\left(y^{(3)} - y^{(1)}\right)\right]^2 + \\ &\left[\left(z^{(2)} - z^{(1)}\right)\left(x^{(3)} - x^{(1)}\right) - \left(x^{(2)} - x^{(1)}\right)\left(z^{(3)} - z^{(1)}\right)\right]^2 + \\ &\left[\left(x^{(2)} - x^{(1)}\right)\left(y^{(3)} - y^{(1)}\right) - \left(y^{(2)} - y^{(1)}\right)\left(x^{(3)} - x^{(1)}\right)\right]^2 \Big\}^{\frac{1}{2}}, \end{aligned} \tag{33}$$

where the superscript '123' denotes the serial numbers of the particles. The surface area of the tetrahedron is $S = S^{(123)} + S^{(124)} + S^{(134)} + S^{(234)}$, and the volume of the tetrahedron can be calculated by

$$V = \frac{1}{6}\begin{vmatrix} x^{(2)} - x^{(1)} & x^{(3)} - x^{(1)} & x^{(4)} - x^{(1)} \\ y^{(2)} - y^{(1)} & y^{(3)} - y^{(1)} & y^{(4)} - y^{(1)} \\ z^{(2)} - z^{(1)} & z^{(3)} - z^{(1)} & z^{(4)} - z^{(1)} \end{vmatrix}. \tag{34}$$

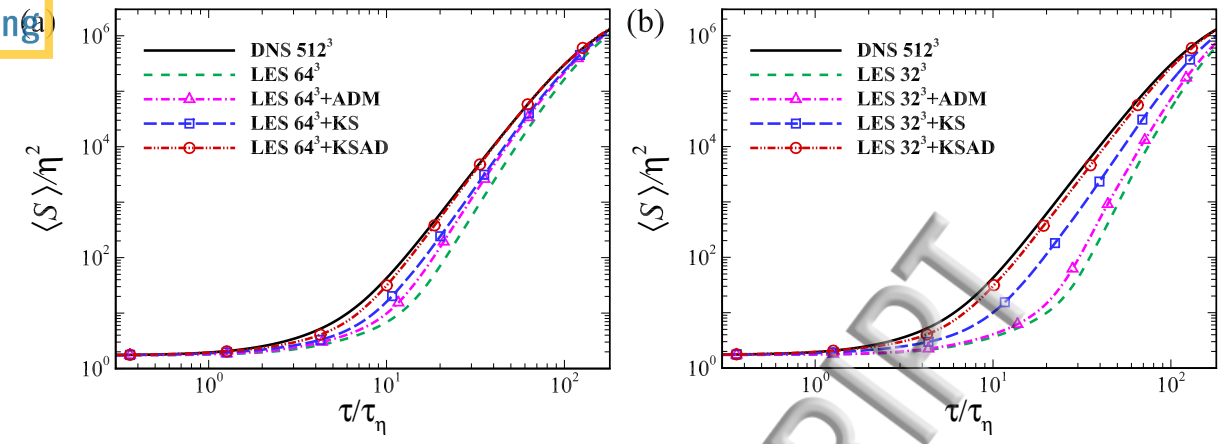

FIG. 12. The mean surface areas of the tetrahedrons from the DNS, LES, and LES with the ADM, KS or KSAD hybrid model.

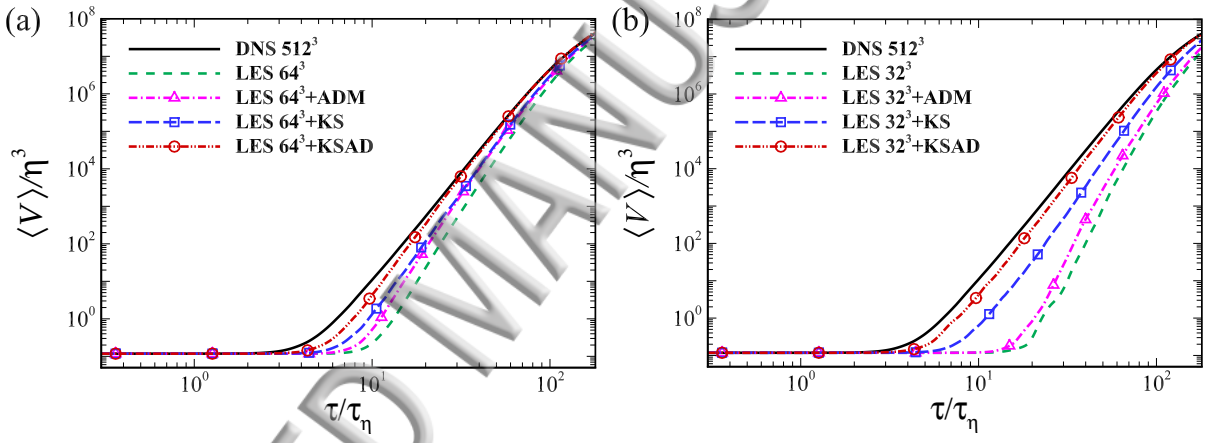

FIG. 13. The mean volumes of the tetrahedrons from the DNS, LES, and LES with the ADM, KS or KSAD hybrid model.

Figs. 12 and 13 show the temporal evolution of the normalized mean surface areas and volumes of the tetrahedrons from the DNS 512^3, conventional LES, and LES with the ADM, KS or KSAD hybrid model, which are denoted by solid lines, dashed lines, dash-dotted lines, long-dashed lines and dash-dot-dotted lines, respectively. In the LES, the flow field is resolved at a coarser grid resolution, and the dissipation by the eddy-viscosity SGS model further reduces the velocity fluctuations. The four-particle dispersion is underpredicted compared to the DNS. The KSAD hybrid model substantially improves the predictions of the mean surface areas and volumes of the tetrahedrons, which is consistent with the prediction of the particle-pair dispersion.

To characterize the shape variation in the tetrahedron, we calculated the renormalized volume and surface area ratios

$$\lambda_V = V/S^{3/2}, \qquad \lambda_S = S/C^2, \tag{35}$$

where C is the perimeter of the tetrahedron. Another indicator of the shape variation in the tetrahedron is the ratio of the intermediate eigenvalue of the inertia matrix $\mathbf{I} = \boldsymbol{\rho}\boldsymbol{\rho}^T$, where

$$\boldsymbol{\rho} = \begin{pmatrix} \rho_x^{(1)} & \rho_x^{(2)} & \rho_x^{(3)} \\ \rho_y^{(1)} & \rho_y^{(2)} & \rho_y^{(3)} \\ \rho_z^{(1)} & \rho_z^{(2)} & \rho_z^{(3)} \end{pmatrix} \tag{36}$$

with $\boldsymbol{\rho}^{(i)} = \left(\rho_x^{(i)}, \rho_y^{(i)}, \rho_z^{(i)}\right)$, $i = 1, 2, 3$, and $\boldsymbol{\rho}^{(1)} = \left(\mathbf{x}^{(2)} - \mathbf{x}^{(1)}\right)/\sqrt{2}$, $\boldsymbol{\rho}^{(2)} = \left(2\mathbf{x}^{(3)} - \mathbf{x}^{(2)} - \mathbf{x}^{(1)}\right)/\sqrt{6}$, $\boldsymbol{\rho}^{(3)} = \left(3\mathbf{x}^{(4)} - \mathbf{x}^{(3)} - \mathbf{x}^{(2)} - \mathbf{x}^{(1)}\right)/\sqrt{12}$. The three eigenvalues of the inertia matrix $\mathbf{I}$ are denoted as g_1, g_2 and g_3 from large to small. Here, we evaluate the variation in the intermediate ratio $I_2 = g_2/(g_1 + g_2 + g_3)$.

In Fig. 14, the temporal evolution of the mean renormalized volume and surface area ratios are shown for the tetrahedrons with an initially regular edge size η. The results from the LES with the KSAD hybrid model show better agreement with the results from the DNS than with the conventional LES. Fig. 15 depicts plots of the temporal evolution of the ratio $\langle I_2 \rangle$ from the DNS, LES, and LES with the ADM, KS or KSAD hybrid model. The deviations of $\langle I_2 \rangle$ between LES and DNS are only partly recovered. Notably, the KSAD hybrid model renders the evolution of the ratio $\langle I_2 \rangle$ from the LES consistent with the result from the DNS.

Finally, we compared the computational costs of the different methods, and further showed the advantage of the hybrid model. Our numerical calculations were performed on the Tianhe-I at the National SuperComputer Center in Tianjin, China. The model of the Central Processing Unit (CPU) is Intel Xeon X5670. Table II shows the number of CPUs and computing time for the different cases. The results indicate that the DNS is very expensive to perform, and the LES is much cheaper. Above all, it takes slightly more computing time to perform the LES plus KSAD hybrid model than the conventional LES. Therefore, the prediction of the Lagrangian dispersion of the fluid particles in the LES is improved by applying the KSAD hybrid model at an acceptable computational cost.

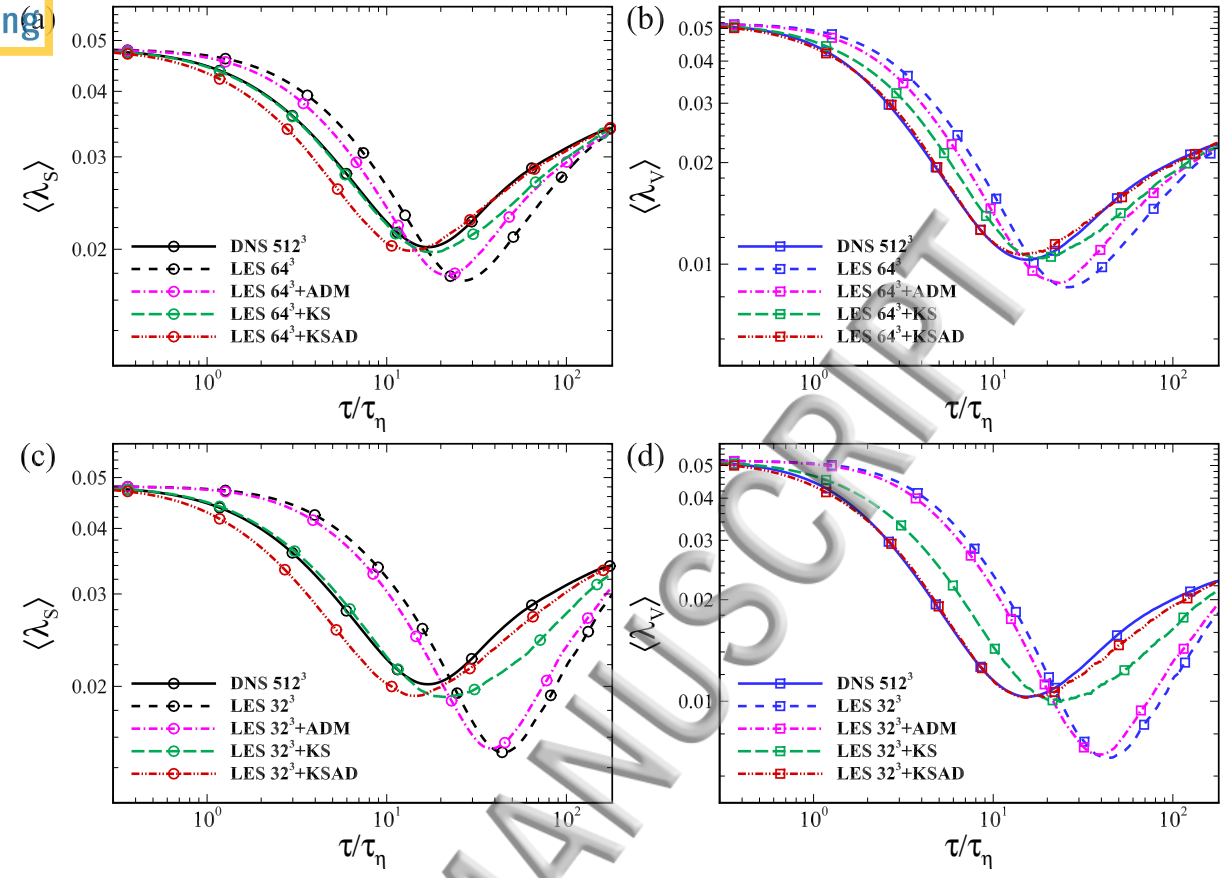

FIG. 14. Temporal evolution of the mean renormalized (a), (c) surface area ratio and (b), (d) volume ratio from the DNS, LES, and LES with the ADM, KS or KSAD hybrid model.

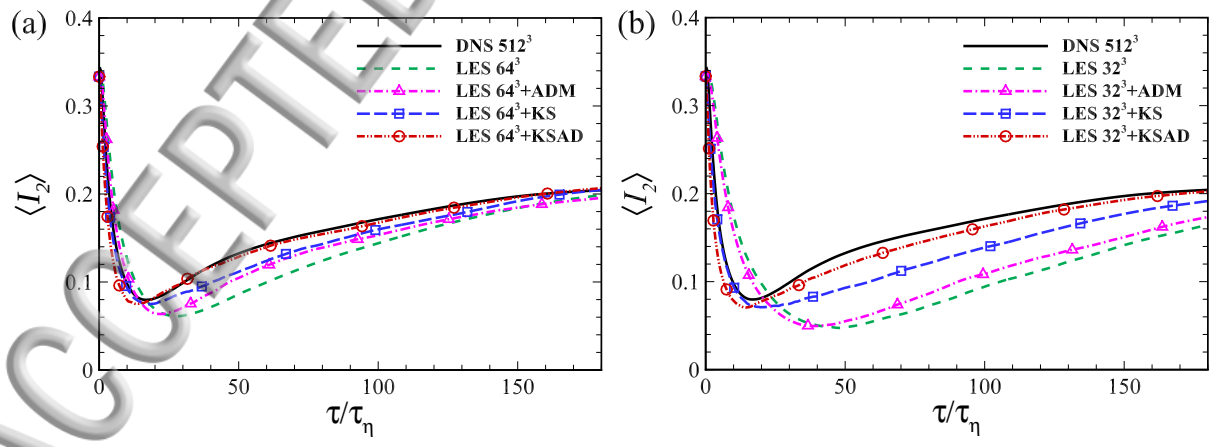

FIG. 15. Temporal evolution of the ratio $\langle I_2 \rangle$ from the DNS, LES, and LES with the ADM, KS or KSAD hybrid model.

TABLE II. The number of CPUs used and the computing time for the different cases. Here, we set $N_p = 50000$. The time intervals from the start of the simulations to the end for all cases are set to $180\tau_\eta$, where τ_η denotes the Kolmogorov time scale.

Case	DNS 512^3	LES 64^3	LES 64^3+KSAD	LES 32^3	LES 32^3+KSAD
Number of CPUs	128	16	16	16	16
Computing time (min)	481.675	4.563	7.142	2.207	4.586

V. CONCLUSION AND PROSPECTIVE

In this work, a KSAD SGS model is developed for predicting the Lagrangian relative dispersion of the fluid particles in the LES of homogeneous and isotropic turbulent flows. Owing to the lack of small-scale motions and SGS model errors, the LES cannot accurately predict the Lagrangian statistics of fluid particles. To improve the predictive capability of the LES, we couple the ADM and KS. After using the ADM, the kinetic energy of the resolved scales in the LES is mostly recovered. Using the KS, the missing SGS velocity fluctuations in the LES are mostly compensated. Then, the Lagrangian statistics of the fluid particles calculated from the LES plus KSAD hybrid model are compared with the corresponding results from the DNS 512^3 and LES. The KSAD hybrid model basically recovers the deviations in the particle pair statistics between the LES and DNS, including the mean and variance of the separation distances, the relative dispersion and one-time two-point Lagrangian velocity correlation functions of the particle pairs. For the four-particle dispersion, the mean surface area and volume of the tetrahedrons, and their renormalized ratios are recovered. In addition, the KSAD hybrid model renders the evolution of $\langle \lambda_V \rangle$, $\langle \lambda_S \rangle$ and $\langle I_2 \rangle$ calculated from the LES consistent with the results from the DNS, which means that the size and topological shape variations in the tetrahedrons are more accurately predicted.

Using the KSAD hybrid model, a significant improvement in the prediction of the Lagrangian dispersion of fluid particles can be achieved for both the LES 64^3 and LES 32^3, in which the grid ratios of the DNS to LES are very large. Moreover, a parametric study is conducted regarding the wavenumbers and orientation wavevectors, and the predictions of particle statistics calculated from the KS formed by different parameters show good agreement with each other. In summary, we can improve the prediction of the Lagrangian

dispersion of fluid particles in the LES of isotropic turbulent flows with a highly coarse grid resolution by only applying a simple KSAD hybrid model at an acceptable additional computational cost.

We shall extend the idea of the KSAD model to flows in more complex geometry in future study. The extension includes three aspects of modifications compared to the isotropic turbulent flows: (I) A more general eddy-viscosity model such as dynamic Smagorinsky model[2], WALE[13], Vreman's model[61], Sigma model[62] or the recent proposed S3PQR model[4] will be used to consider the effects of walls and get the nonhomogeneous turbulent flows at large scales. (II) The approximate deconvolution method based on elliptical differential filters is used for solid boundary conditions[38,39]. Park et al.[37] used a dynamic model based on elliptical differential filters as the approximate deconvolution method for the LES of particle-laden turbulent flows to model the subgrid-scale velocity and describe the motion of the small inertial particles. This model is flexible to be used in any type of flow configurations. (III) The Gabor transform can be used to the conventional Fourier modes to localize the Fourier modes. To account for inhomogeneities at large-scale in wall-bounded flows, we can assume the local homogeneity in a small region and the Gabor transform can be used to the conventional Fourier modes to localize the Fourier modes. Ghate and Lele[63] used the Fourier-Gabor mode to recover the subgrid-scale turbulent flows in the planetary boundary layer (PBL) and a finite Reynolds number channel flow.

ACKNOWLEDGMENTS

This work was supported by Science Challenge Program (JCKY2016212A501), the National Natural Science Foundation of China (11472277, 11572331 and 11772337), Strategic Priority Research Program, CAS (XDB22040104), Key Research Program of Frontier Sciences, CAS (QYZDJ-SSW-SYS002).

REFERENCES

[1]P. Moin and K. Mahesh, "Direct numerical simulation: A tool in turbulence research," Annu. Rev. Fluid Mech. **30**, 539–578 (1998).

[2]M. Germano, U. Piomelli, P. Moin, and W. H. Cabot, "A dynamic subgrid-scale eddy viscosity model," Phys. Fluids **A3**, 1760 (1991).

[3]F. Dabbagh, F. X. Trias, A. Gorobets, and A. Oliva, "A priori study of subgrid-scale features in turbulent Rayleigh-Benard convection," Phys. Fluids **29**, 105103 (2017).

[4]F. X. Trias, D. Folch, A. Gorobets, and A. Oliva, "Building proper invariants for eddy-viscosity subgrid-scale models," Phys. Fluids **27**, 065103 (2015).

[5]F. X. Trias, A. Gorobets, M. H. Silvis, R. W. C. P. Verstappen, and A. Oliva, "A new subgrid characteristic length for turbulence simulations on anisotropic grids," Phys. Fluids **29**, 115109 (2017).

[6]C. P. Yu, Z. L. Xiao, and X. L. Li, "Dynamic optimization methodology based on subgrid-scale dissipation for large eddy simulation," Phys. Fluids **28**, 015113 (2016).

[7]C. P. Yu, Z. L. Xiao, and X. L. Li, "Scale-adaptive subgrid-scale modelling for large-eddy simulation of turbulent flows," Phys. Fluids **29**, 035101 (2017).

[8]M. H. Silvis, R. A. Remmerswaal, and R. Verstappen, "Physical consistency of subgrid-scale models for large-eddy simulation of incompressible turbulent flows," Phys. Fluids **29**, 015105 (2017).

[9]A. Vollant, G. Balarac, and C. Corre, "A dynamic regularized gradient model of the subgrid-scale stress tensor for large-eddy simulation," Phys. Fluids **28**, 025114 (2016).

[10]O. Thiry and G. Winckelmans, "A mixed multiscale model better accounting for the cross term of the subgrid-scale stress and for backscatter," Phys. Fluids **28**, 025111 (2016).

[11]S. AL-Bairmani, Y. Li, C. Rosales, and Z. T. Xie, "Subgrid-scale stresses and scalar fluxes constructed by the multi-scale turnover Lagrangian map," Phys. Fluids **29**, 045103 (2017).

[12]S. Schneiderbauer and M. Saeedipour, "Approximate deconvolution model for the simulation of turbulent gas-solid flows: An a priori analysis," Phys. Fluids **30**, 023301 (2018).

[13]F. Nicoud and F. Ducros, "Subgrid-scale stress modelling based on the square of the velocity gradient tensor," Flow, Turbul. Combust. **62**, 183–200 (1999).

[14]V. Armenio, U. Piomelli, and V. Fiorotto, "Effect of the subgrid scales on particle motion," Phys. Fluids **11**, 3030 (1999).

[15]C. Marchioli, M. V. Salvetti, and A. Soldati, "Some issues concerning large-eddy simulation of inertial particle dispersion in turbulent bounded flows," Phys. Fluids **20**, 040603 (2008).

[16]Y. Yang, G. W. He, and L. P. Wang, "Effects of subgrid-scale modeling on Lagrangian

tatistics in large eddy simulation," J. Turbul. **9**, 1–24 (2008).

[17]G. D. Jin, G. W. He, and L. P. Wang, "Large-eddy simulation of turbulent collision of heavy particles in isotropic turbulence," Phys. Fluids **22**, 055106 (2010).

[18]B. Ray and L. R. Collins, "A subgrid model for clustering of high-inertia particles in large-eddy simulations of turbulence," J. Turbul. **15**, 366–385 (2014).

[19]J. C. Chen and G. D. Jin, "Large-eddy simulation of turbulent preferential concentration and collision of bidisperse heavy particles in isotropic turbulence," Powder Technol. **314**, 281–290 (2017).

[20]C. Marchioli, "Large-eddy simulation of turbulent dispersed flows: a review of modelling approaches," Acta Mech. **228**, 741–771 (2017).

[21]Z. D. Zhou, J. C. Chen, and G. D. Jin, "Prediction of Lagrangian dispersion of fluid particles in isotropic turbulent flows using large-eddy simulation method," Acta Mech. **228**, 3203–3222 (2017).

[22]B. J. Geurts, "Inverse modeling for large-eddy simulation," Phys. Fluids **9**, 3585 (1997).

[23]S. Stolz and N. A. Adams, "An approximate deconvolution procedure for large-eddy simulation," Phys. Fluids **11**, 1699 (1999).

[24]S. Stolz, N. A. Adams, and L. Kleiser, "An approximate deconvolution model for large-eddy simulation with application to incompressible wall-bounded flows," Phys. Fluids **13**, 997 (2001).

[25]S. K. Das and P. A. Durbin, "A Lagrangian stochastic model for dispersion in stratified turbulence," Phys. Fluids **17**, 025109 (2005).

[26]J. Pozorski and S. V. Apte, "Filtered particle tracking in isotropic turbulence and stochastic modeling of subgrid-scale dispersion," Int. J. Multiphase Flow **35**, 118–128 (2009).

[27]R. H. Kraichnan, "Diffusion by a random velocity field," Phys. Fluids **13**, 22 (1970).

[28]J. C. H. Fung, J. C. R. Hunt, N. A. Malik, and R. J. Perkins, "Kinematic simulation of homogeneous turbulence by unsteady random Fourier modes," J. Fluid Mech. **236**, 281–318 (1992).

[29]J. C. H. Fung and J. C. Vassilicos, "Two-particle dispersion in turbulentlike flows," Phys. Rev. E **57**, 1677–1690 (1998).

[30]C. Marchioli, M. V. Salvetti, and A. Soldati, "Appraisal of energy recovering sub-grid scale models for large-eddy simulation of turbulent dispersed flows," Acta Mech. **201**, 277–296 (2008).

[31]G. Gobert and M. Manhart, "Subgrid modelling for particle-LES by spectrally optimised interpolation (SOI)," J. Comput. Phys. **230**, 7796–7820 (2011).

[32]J. G. M. Kuerten, "Subgrid modeling in particle-laden channel flow," Phys. Fluids **18**, 025108 (2006).

[33]B. Shotorban and F. Mashayek, "Modeling subgrid-scale effects on particles by approximate deconvolution," Phys. Fluids **17**, 081701 (2005).

[34]B. Shotorban, K. K. Q. Zhang, and F. Mashayek, "Improvement of particle concentration prediction in large-eddy simulation by defiltering," Int. J. Heat Mass Tran. **50**, 3728–3739 (2007).

[35]G. D. Jin and G. W. He, "A nonlinear model for the subgrid timescale experienced by heavy particles in large eddy simulation of isotropic turbulence with a stochastic differential equation," New J. Phys. **15**, 035011 (2013).

[36]G. W. He, G. D. Jin, and Y. Yang, "Space-time correlations and dynamic coupling in turbulent flows," Annu. Rev. Fluid Mech. **49**, 51–70 (2017).

[37]G. I. Park, M. Bassenne, J. Urzay, and P. Moin, "A simple dynamic subgrid-scale model for LES of particle-laden turbulence," Phys. Rev. Fluids **2**, 044301 (2017).

[38]M. Germano, "Differential filters for the large eddy numerical-simulation of turbulent flows," Phys. Fluids **29**, 1755 (1986).

[39]M. Germano, "Differential filters of elliptic type," Phys. Fluids **29**, 1757 (1986).

[40]M. S. Borgas and B. L. Sawford, "A family of stochastic models for two-particle dispersion in isotropic homogeneous stationary turbulence," J. Fluid Mech. **279**, 69–99 (1994).

[41]G. Pedrizzetti and E. A. Novikov, "On Markov modelling of turbulence," J. Fluid Mech. **280**, 69–93 (1994).

[42]B. M. O. Heppe, "Generalized Langevin equation for relative turbulent dispersion," J. Fluid Mech. **357**, 167–198 (1998).

[43]D. J. Thomson, "Criteria for the selection of stochastic models of particle trajectories in turbulent flows," J. Fluid Mech. **180**, 529–556 (1987).

[44]O. Simonin, E. Deutsch, and J. P. Minier, "Eulerian prediction of the fluid/particle correlated motion in turbulent two-phase flows," Appl. Sci. Res. **51**, 275–283 (1993).

[45]D. J. Thomson, "A stochastic model for the motion of particle pairs in isotropic high-Reynolds-number turbulence, and its application to the problem of concentration variance," J. Fluid Mech. **210**, 113–153 (1990).

[46]O. A. Kurbanmuradov, "Stochastic Lagrangian models for two-particle relative dispersion in high-Reynolds number turbulence," Monte Carlo Methods Appl. **3**, 37–52 (1997).

[47]B. J. Devenish, "Geometrical properties of turbulent dispersion," Phys. Rev. Lett. **110**, 064504 (2013).

[48]I. M. Mazzitelli, F. Toschi, and A. S. Lanotte, "An accurate and efficient Lagrangian sub-grid model," Phys. Fluids **26**, 095101 (2014).

[49]D. R. Osborne, J. C. Vassilicos, and J. D. Haigh, "One-particle two-time diffusion in three-dimensional homogeneous isotropic turbulence," Phys. Fluids **17**, 035104 (2005).

[50]D. J. Thomson and B. J. Devenish, "Particle pair separation in kinematic simulations," J. Fluid Mech. **526**, 277–302 (2005).

[51]H. D. Yao and G. W. He, "A kinematic subgrid scale model for large-eddy simulation of turbulence-generated sound," J. Turbul. **10**, 1–14 (2009).

[52]T. Sadd, D. Cline, R. Stoll, and J. C. Sutherland, "Scalable tools for generating synthetic isotropic turbulence with arbitrary spectra," AIAA J. **55**, 327–331 (2017).

[53]N. A. Malik and J. C. Vassilicos, "A Lagrangian model for turbulent dispersion with turbulent-like flow structure: Comparison with direct numerical simulation for two-particle statistics," Phys. Fluids **11**, 1572 (1999).

[54]P. K. Yeung, "Direct numerical simulation of two-particle relative diffusion in isotropic turbulence," Phys. Fluids **6**, 3416 (1994).

[55]P. Flohr and J. C. Vassilicos, "A scalar subgrid model with flow structure for large-eddy simulations of scalar variances," J. Fluid Mech. **407**, 315–349 (2000).

[56]W. R. Michałek, J. G. M. Kuerten, J. C. H. Zeegers, R. Liew, J. Pozorski, and B. J. Geurts, "A hybrid stochastic-deconvolution model for large-eddy simulation of particle-laden flow," Phys. Fluids **25**, 123302 (2013).

[57]J. C. Chen, G. D. Jin, and J. Zhang, "Lagrangian statistics in isotropic turbulent flows with deterministic and stochastic forcing schemes," Acta Mech. Sinica **31**, 25–31 (2015).

[58]J. P. Chollet and M. Lesieur, "Parameterization of small scales of three-dimensional isotropic turbulence utilizing spectral closure," J. Atmos. Sci. **38**, 2747–2757 (1981).

[59]J. P. Chollet, "Two-point closure used for a sub-grid scale model in large eddy simulations," Springer, Berlin **Turbulent Shear Flow 4**, 62–72 (1985).

[60]S. B. Pope, *Turbulent flows* (Cambridge University Press, Cambridge, 2000).

[61]A. W. Vreman, "An eddy-viscosity subgrid-scale model for turbulent shear flow: Algebraic

theory and applications," Phys.Fluids **16**, 3670 (2004).

[62]F. Nicoud, H. B. Toda, O. Cabrit, S. Bose, and J. Lee, "Using singular values to build a subgrid-scale model for large eddy simulations," Phys. Fluids **23**, 085106 (2011).

[63]A. S. Ghate and S. K. Lele, "Subfilter-scale enrichment of planetary boundary layer large eddy simulation using discrete Fourier-Gabor modes," J. Fluid Mech. **819**, 494–539 (2017).